MODELING REVEALS CORTICAL DYNEIN REGULATION OF SPINDLE BIPOLARITY

A PREPRINT

Dayna Mercadante
Bioinformatics and Computational Biology Program
Worcester Polytechnic Institute
Worcester, MA 01609 USA
damercadante@wpi.edu

Amity Manning
Department of Biology and Biotechnology
Worcester Polytechnic Institute
Worcester, MA 01609 USA
almanning@wpi.edu

Sarah Olson
Department of Mathematical Sciences
Worcester Polytechnic Institute
Worcester, MA 01609 USA
sdolson@wpi.edu

July 10, 2020

ABSTRACT

Proper formation and maintenance of the mitotic spindle is required for faithful cell division. While much work has been done to understand the roles of the key force components of the mitotic spindle, identifying the implications of force perturbations in the spindle remains a challenge. We developed a computational framework of the minimal force requirements for mitotic progression and used experimental approaches to further define and validate the model. Through simulations, we show that rather than achieving and maintaining a constant bipolar spindle length, oscillations in pole to pole distance occur that coincide with microtubule binding and force generation by cortical dynein. In the context of high kinesin-14 (HSET) activity, we reveal the requirement of high cortical dynein activity for bipolar spindle formation.

1 Introduction

Mathematical and computational modeling of biological processes can bypass experimental limitations and provide a framework to identify and manipulate individual molecular components. An appealing candidate for such modeling is the process of cell division, during which the mitotic spindle forms and is responsible for separating the genetic material of a cell into two identical daughter cells. The spindle is a biophysical machine that is composed of microtubules (MTs) organized about two centrosomes, the organelles responsible for MT nucleation [1]. MTs are oriented such that their plus-ends, those that dynamically grow and shrink [2], point outward while their minus ends remain anchored at the centrosome [3, 4, 5]. This orientation of MTs generates a radial array called a spindle pole. As mitosis proceeds, the mitotic spindle forms and maintains a bipolar configuration, with the two centrosomes positioned at opposite sides of the cell.

Bipolar spindle formation is orchestrated by the activity of motor proteins, which walk along MTs in a directional fashion (plus- or minus-end directed) [6, 7, 8, 9, 10]. Proper formation of the mitotic spindle is required for accurate chromosome segregation, and while the molecular regulation of segregation onset is dependent on stable MT attachments to chromosomes [11], chromosomes are dispensable for bipolar spindle assembly [12, 13, 14]. To better understand the key mechanistic requirements of bipolar spindle formation and maintenance, we developed a simplified computational model of the mammalian mitotic spindle. Our model includes forces driving centrosome movement by MT interactions with three motor proteins: kinesin-5 (Eg5), kinesin-14 (HSET), and dynein, and excludes forces derived from MT interactions with chromosomes. Results from the model indicate that dynein activity at the cell cortex directly impacts

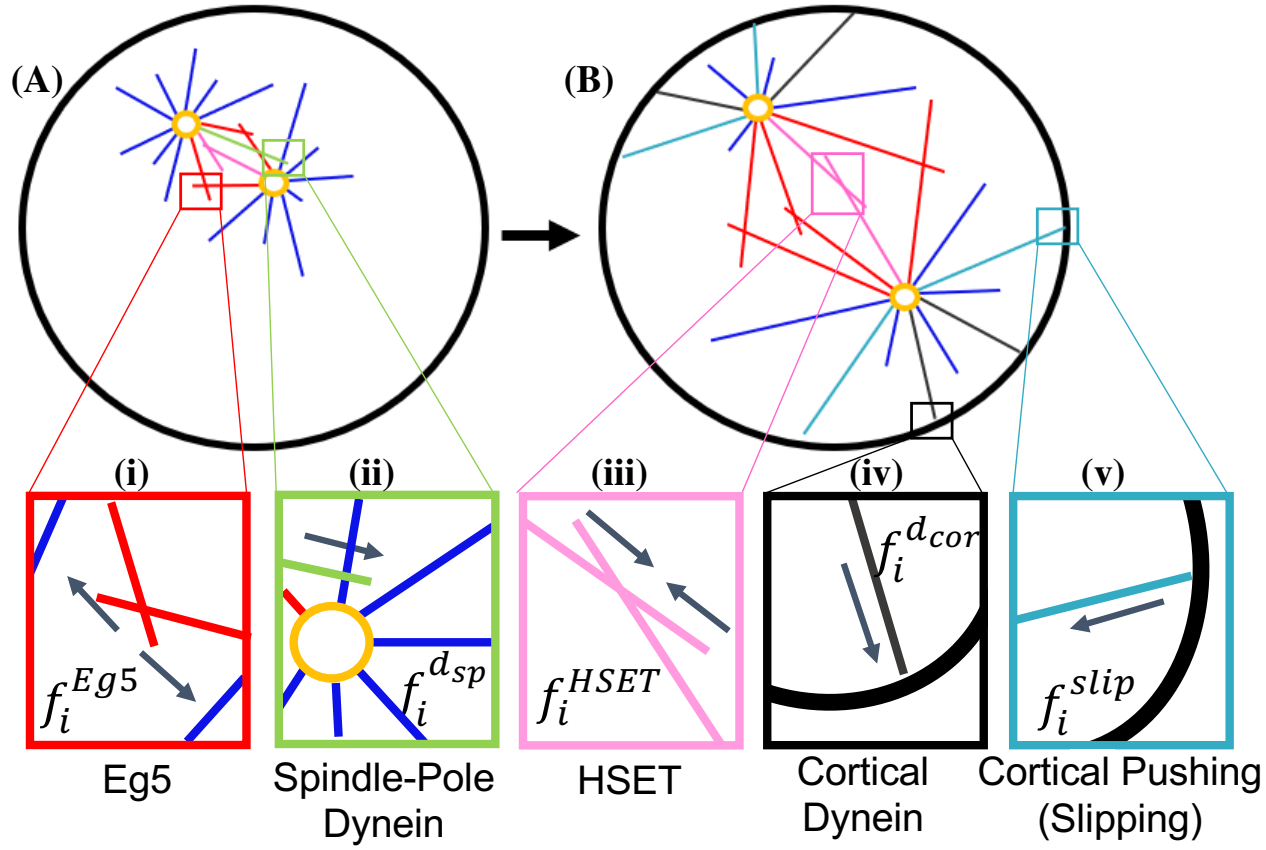

Figure 1: **MT-associated forces are involved in forming and maintaining a bipolar spindle in the absence of chromosome interactions**. A balance of pushing and pulling forces are required for proper centrosome separation in (A) and maintenance of spindle bipolarity in (B). (i) Eg5 pushes centrosomes apart by generating force at antiparallel MT overlap regions. (ii) Dynein localized to spindle poles binds to and pulls MTs from the opposing spindle pole. (iii) HSET pulls centrosomes together by generating force at antiparallel MT overlap regions. (iv) Dynein localized to the cell cortex bound to MTs pulls the centrosome towards the boundary. (v) MTs growing and slipping against the cell cortex push the centrosome away from the boundary.

both bipolar spindle length and oscillations in pole to pole distance over time. Results further reveal that cortical dynein activity is required for bipolar spindle formation in the context of HSET overexpression.

2 Methods

2.1 Model Overview

The mitotic spindle has been appealing to biologists, mathematicians, and physicists alike for decades [15]. Many models have been developed to understand early centrosome separation and spindle formation [16, 17, 18, 19, 20, 21, 22, 23], chromosomes dynamics, [24, 25, 26, 27, 28, 29], and spindle elongation during anaphase [30, 31, 32]. Biological interpretation is dependent on parameters and assumptions, making applications to mammalian cells challenging since their spindle and genome are more complex than those of embryos or yeast.

We developed a minimal computational model to analyze centrosome movement and mammalian mitotic spindle formation in the absence of chromosomes, benchmarked on previous *in vitro* assays and modeling approaches that capture dynamic centrosome positioning and cell division [33, 34, 21] (Appendices A, B). Analysis of individual force components over time makes this model distinct from previously published models that do not explore time-dependent changes in forces or their relationship to spindle dynamics. In our 2-dimensional simulations, the cell cortex is a rigid, circular boundary, with a diameter of 30 μm, capturing a mammalian cell that has rounded as it enters mitosis

[35, 36, 37]. We consider MT-motor protein derived forces that are responsible for centrosome movement and bipolar spindle formation. Where available, experimentally defined parameters using mammalian cell culture were chosen from the literature, and all parameters described below are listed in Table 2.

2.1.1 Motor Proteins

We consider three different force-generating motor proteins in the system; all are stochastic and based on geometric constraints.

Dynein is a minus-end directed motor that is localized to two distinct regions during mitosis: at spindle poles (sp) where it maintains MT minus-end focusing and is essential for spindle pole integrity [38, 39, 40, 41], and at the cell cortex (cor) where it binds to MT plus-ends and pulls centrosomes towards the boundary of the cell [42, 17, 43, 33, 34, 44, 45]. We consider these populations to be distinct and generate forces, $f_i^{d_{sp}}$ and $f_i^{d_{cor}}$, respectively, on MT i (Figure 1 ii,iv, Appendix A, Equation 2,9).

Kinesin-5 (Eg5) is a plus-end directed motor protein that generates force on two antiparallel MTs. This force is necessary for centrosome separation early in mitosis, as loss of Eg5 prevents centrosome separation and results in monopolar spindles [9, 46, 47, 48]. Binding of Eg5 also stabilizes MT plus-ends [49]. To model this behavior in our simulations, MTs that are bound to Eg5 continue to grow from their plus-ends but cease to undergo catastrophe. Eg5-dependent forces acting at antiparallel MT overlap regions are f_i^{Eg5}, f_j^{Eg5} on MTs i, j nucleated from centrosomes c, k, respectively (Figure 1 i, Appendix A, Equation 6).

Kinesin-14 (HSET) is a minus-end directed motor that crosslinks and generates force on two antiparallel MTs. This force is antagonistic to Eg5 and contributes to spindle maintenance during mitosis [14, 40]. We consider MTs bound to HSET to have stabilized plus-ends, similar to those bound to Eg5. The forces by HSET acting at antiparallel MT overlap regions are f_i^{HSET}, f_j^{HSET} (Figure 1 iii, Appendix A, Equation 7).

2.1.2 Non-Motor Protein Derived Force

MTs that interact with the cell cortex but do not bind to dynein can continue to grow and slip along the cell cortex, generating a force against the MT and pushing the centrosome away from the boundary [33, 50]. We consider this force at MT plus-ends as f_i^{slip} on MT i (Figure 1 v, Appendix A, Equation 4).

2.1.3 Centrosome Movement

Considering the above mentioned forces derived by MTs and motor protein interactions, our system of force-balance equations for the movement of centrosome c in the overdamped limit is:

$$\vec{0} = \vec{F}_c^{d_{cor}} + \vec{F}_c^{slip} + \vec{F}_c^{Eg5} + \vec{F}_c^{HSET} + \vec{F}_c^{d_{sp}} + \vec{F}_c^{r_{cent}} + \vec{F}_c^{r_{cor}} + \xi\vec{v_c}, \tag{1}$$

where $\vec{F}_c^{\beta} = \sum_{i=1}^{N_c} f_i^{\beta} S_i^{\beta} \vec{m}_i$, $\beta = d_{cor}, slip, Eg5, HSET, d_{sp}$ are forces generated by MTs i in the direction $\vec{m}_i$, nucleated from centrosome c, and S_i is a scaling factor that is dependent on MT length (Appendix A). We consider additional repulsive forces; $\vec{F}_c^{r_{cent}} = \frac{\vec{V}_{cent}C}{d_{cent}}$, which prevents two centrosomes from occupying the same space, and $\vec{F}_c^{r_{cor}} = \frac{\vec{V}_{cor}C}{d_{cor}}$ which prevents a centrosome from overlapping with the boundary. $\vec{V}_{cent}$ is the vector between centrosomes (Appendix A, Figure A2 A) while $\vec{V}_{cor}$ is the vector between the centrosome and the closest point on the cell cortex. d_{cent} is the distance between centrosomes, d_{cor} is the minimal distance between centrosome c and the cell cortex, and C is a scaling factor. We solve a system of c equations for the velocity of each centrosome, $\vec{v}_c$, and use the velocity to determine the new location of each centrosome. The velocity is scaled by a drag coefficient, ξ, to account for the viscosity of the cytoplasm within the cell. The value of ξ is calculated by $\mu/\sqrt{(\gamma)}$ where μ is the viscosity and γ is the permeability, approximated using the volume fraction of MTs in the system [51]. Our drag coefficient captures appropriate mitotic timing, as increasing drag delays centrosome separation and spindle formation (Supplemental Figure S1).

2.2 Model Analysis

Simulations and model analysis was performed in MATLAB. The base case of the model considered all parameters listed in Table 2, and was validated by centrosome movement when a single centrosome is

present (Appendix B). To observe the stochasticity in the model by MT dynamics and MT-motor protein binding and unbinding, we performed 10 simulations with the same initial centrosome positioning. Traces of centrosome movement over time show different initial trajectories (Supplementary Figure S2 A), but the velocity of centrosomes and the distance between centrosomes (spindle length) have similar trends (Supplementary Figure S2 B). Since we are primarily interested in spindle length, we determined the required number of simulations to accurately represent model results by quantifying the average final spindle length (at t=25 min) for 10, 20, 30, and 40 simulations with random initial centrosome positioning of the base case (Table 1). This analysis indicates that the average final spindle length does not change with additional simulations.

Table 1: Average (Avg) Spindle Length for Simulations (Sims) at t=25 min.

# of Sims	Avg length (μm)
10	16.37
20	16.32
30	16.33
40	16.37

Simulations achieving spindle bipolarity were those having a spindle length of at least 15 μm (the average bipolar spindle length in cells lacking stable chromosome attachments (Figure 2 C)) at t=25 min. Monopolar spindles were characterized by spindle length being less than half the average bipolar spindle length (7.5 μm) at t=25 min.

2.3 Cell Culture, siRNA, Cell Line Generation

hTERT-immortaized Retinal Pigment Epithelial (RPE) cells were maintained in Dulbecco's Modified Essential Medium (DMEM) supplemented with 10% fetal bovine serum (FBS) and 1% Penicillin and Streptomycin and maintained at 37°C with 5% CO_2. Depletion of Nuf2 was achieved by transient transfection of a pool of four siRNA constructs (target sequences 5'-gaacgaguaaccacaauua-3', 5'-uagcugagauugugauuca-3', 5'-ggauugcaauaaaguucaa-3', 5'-aaacgauagugcugcaaga-3') at 50 nM using RNAiMAX transfection reagent according to manufacturer's instructions. Nuf2 makes up one of the four arms of the Ndc80 complex, which attaches MTs to kinetochores, along with Hec1, Spc24, and Spc25 [52]. Hec1 and Nuf2 dimerize in this complex, and knockdown of either protein destabilizes the other complex member, leading to loss of MT attachments to kinetochores [53]. Therefore, knockdown of Nuf2 was confirmed using immunofluorescence imaging with antibodies specific for Hec1 (Novus Biologicals) to assess kinetochore localization of the complex.

RPE cells stably expressing L304-EGFP-Tubulin (Addgene #64060) were generated by lentiviral transduction and placed under 10 μg/mL puromycin selection for 5-7 days. Expression of the tagged construct was confirmed by immunofluorescent imaging [54].

2.4 Immunofluorescence Imaging

Cells were captured with a Zyla sCMOS camera mounted on a Nikon Ti-E microscope. A 60x Plan Apo oil immersion objective was used for fixed-cell imaging and live-cell imaging of RPE cells expressing GFP-centrin to visualize centrosomes [55], and a 20x CFI Plan Fluor objective was used for live-cell imaging of RPE cells expressing GFP-tubulin [54].

2.5 Fixed-cell Imaging and Analysis

Cells seeded onto glass coverslips were rinsed briefly in phosphate buffered saline (PBS) and placed in ice cold methanol for 10 minutes at -20°C. Coverslips were washed briefly with PBS and blocked in TBS-BSA (10 mM Tris at pH 7.5, 150 mM NaCl, 1% bovine serum albumin (BSA)) for 10 minutes. Cells were incubated with primary antibodies diluted in TBS-BSA (anti-α-tubulin (1:1500; Abcam ab18251), anti-Ndc80 (1:500; Novus Biologicals)) for 1 hour in a humid chamber. Cells were washed in TBS-BSA for 10 minutes then incubated with secondary antibodies diluted 1:1000 in TBS-BSA + 0.2 μg/mL DAPI for 45 minutes.

Fixed and live-cell image analysis was performed in NIS Elements. Fixed cell analysis of DNA area was quantified by gating a region of interest by DAPI fluorescence intensity. Spindle length was quantified by performing line scans along the long axis of the mitotic spindle and considering the spindle poles to be the two highest peaks in fluorescence intensity. Spindle morphology was characterized as bipolar, monopolar, or disorganized, where monopolar spindles were characterized by spindle length being less than half the average bipolar spindle length, and disorganized spindles had indistinguishable spindle poles. All representative images are of a single focal plane. Background was removed and contrast was adjusted in ImageJ for fixed-cell and GFP-centrin live-cell images. Statistical analysis was performed in Excel; two-tailed Student's *t*-test was used for comparisons between two groups.

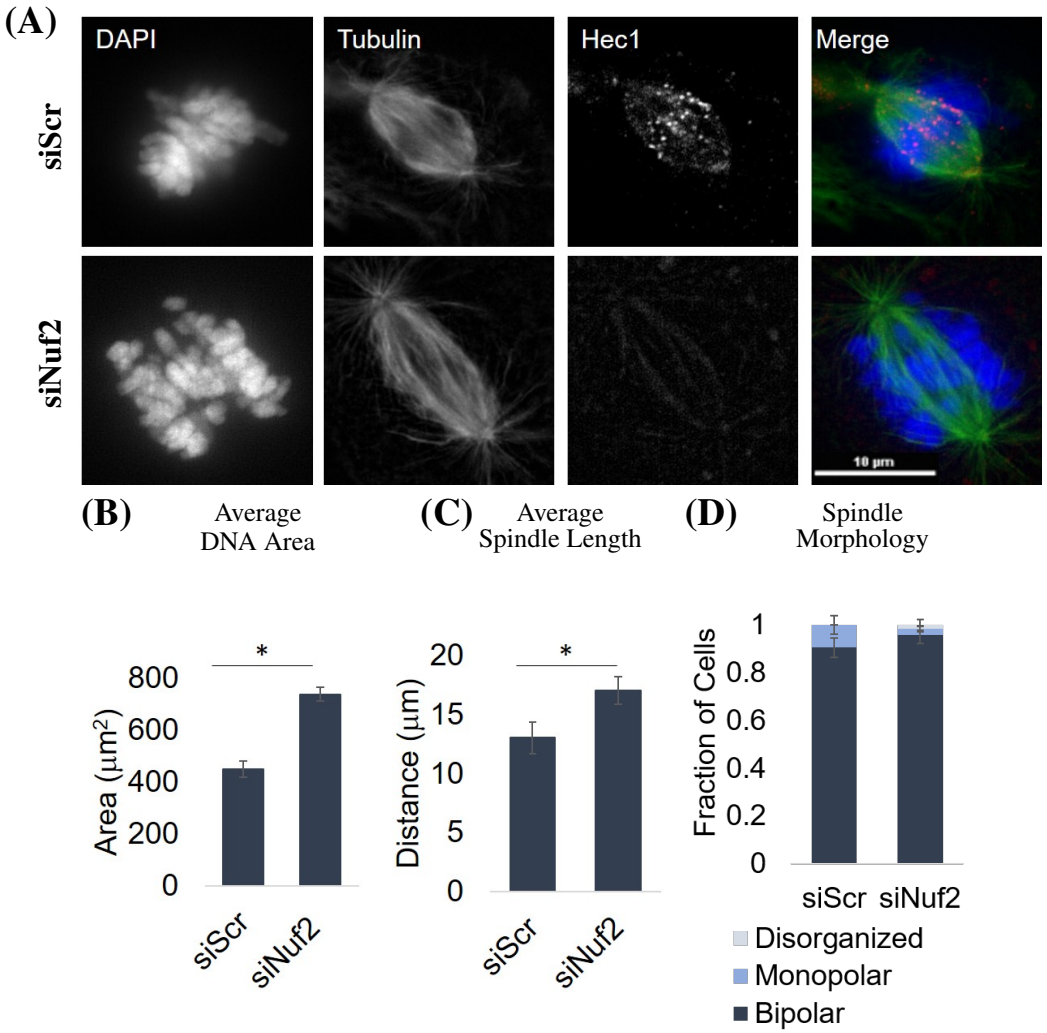

Figure 2: **Stable end-on kinetochore attachments are not required for bipolar spindle formation.** (A) Fixed-cell imaging of RPE cells stained for DAPI (DNA), Tubulin (MTs), and Hec1 (NDC80) in the control (siScr) and knockdown (siNuf2) condition. (B) Quantification of the average DAPI area in the control (siScr) and knockdown (siNuf2) condition. (C) Quantification of the average spindle length in the control (siScr) and knockdown (siNuf2) condition. (D) Quantification of the average fraction of cells with bipolar, monopolar, or disorganized spindles. All averages calculated from at least 30 cells from 3 biological replicates. Error bars are standard deviation (SD). *p<0.05 indicates statistical significance.

2.6 Live-cell Imaging

RPE cells stably expressing α-tubulin-EGFP were seeded onto a 6-well plate. NIS elements HCA jobs software was used to enable multi-coordinate, multi-well imaging in a single z-stack (0.67 μm per pixel) [54]. Images were captured every 5 minutes for 16 hours. Analysis was performed on at least 40 mitotic cells.

RPE cells stably expressing GFP-centrin were seeded onto glass coverslips and placed in a sealed chamber slide with 100 μl of media. Single cells entering mitosis were captured at 60x in a single z-stack (0.11 μm per pixel) every minute for the duration of mitosis.

3 Results/Discussion

3.1 Chromosomes are dispensable for spindle formation and maintenance

To inform our model and better define the extent to which chromosome attachments are dispensable for normal spindle structure, we performed fixed-cell image analysis of RPE cells depleted of Nuf2 (siNuf2), a protein essential for MT binding to kinetochores (Figure 2 A). RPE cells are a well characterized, diploid, immortalized mammalian cell line; a useful tool for mitotic analysis. Consistent with previously described work [12, 13, 14], we find that Nuf2 depletion leads to a marked decrease in Hec1 localization at kinetochores, dispersion of chromosomes throughout the cell, and an increase in spindle length compared to the control condition, indicating failure to form stable MT attachments to kinetochores (Figure 2 B,C). Despite these differences, spindle morphology remains largely bipolar in the Nuf2 depleted condition, with more than 90% of cells achieving bipolarity (Figure 2 D). These data suggests that chromosomes and chromosome-derived forces are not required for bipolar spindle formation and maintenance.

3.2 A biophysical model captures bipolar spindle formation and maintenance.

To further define model requirements and validate model outputs, we performed live-cell imaging of RPE cells stably expressing a GFP-α-tubulin transgene (Figure 3 A). Since centrosomes are linked to spindle poles by molecular mechanisms [66, 41], we use this imaging, in addition to live-cell imaging of RPE cells expressing a GFP-tagged centrosome marker (GFP-centrin) (Figure 3 F,G), to observe and quantify centrosome movement over time. To inform initial conditions of the model, we quantified intracentrosomal distances just prior to nuclear envelope breakdown (NEB), defined as the first point in time at which GFP-tubilin is no longer visibly excluded from the nuclear region. This analysis reveals a wide distribution, with initial centrosome distances ranging between 2.5 and 22.2 μm (Figure 3 C). To mirror this distribution of centrosome positions in our model, we initialize centrosomes to be randomly placed at least 7.5 μm from the center of the cell, achieving a range of distances between 3.2 and 15.9 μm (Figure 3 C).

Live-cell imaging was used to monitor centrosome movement and spindle bipolarity, revealing that 40% of cells achieve spindle bipolarity by 5 min and 96% by 10 min (Figure 3 D). Imaging analyses also capture centrosome separation at early time points (Figure 3 E,F,G(i)) until an eventual bipolar spindle is achieved and maintained at an average spindle length of 12 μm (Figure 3 E). These results are consistent with fixed-cell image analysis of RPE cells with stable MT-chromosome attachments in Figure 2 C (siScr). By tracking individual centrosome positions in time, we calculate that they have a velocity less than 0.1 μm/sec.

Our model captures appropriate mitotic timing, with 40% of simulations achieving spindle bipolarity by 5 min and 100% by 10 min. (Figure 3 D). The model achieves an average bipolar spindle length of 15 μm (Figure 3 E), consistent with with fixed-cell image analysis of cells lacking stable MT-chromosome attachments in Figure 2 C (siNuf2). Traces of centrosome movement and centrosome velocity over time similarly resemble the biological data (Figure 3 G,H), validating the use of our biophysical model as a tool to further understand the dynamics of mitotic spindle formation and maintenance.

3.3 Motor protein perturbations alter spindle bipolarity

The mitotic spindle has been extensively studied, and our understanding of the force requirements for spindle bipolarity has been determined primarily through experimental manipulation of force-generating motor proteins. While informative, biological assays can induce potential off-target effects that impact multiple cellular processes. To determine how motor proteins considered in our model impact spindle bipolarity, we independently perturbed motor function of Eg5, HSET, and cortical dynein by altering the binding probability of the motor β from its base case of $P_\beta = 0.5$ to $P_\beta = 0$ (Table 2, Appendix A).

Biological data indicates that loss of Eg5 activity results in spindle pole collapse and the formation of a monopolar spindle [48]. To replicate Eg5 loss in the model, the Eg5 binding probability to MTs (P_E) was set to zero. Consistent with *in vivo* data, our simulations with loss of Eg5 activity results in rapid spindle pole collapse (Figure 4 A(i),D. In the base case of our model, dynein localized to spindle poles is dispensable for spindle bipolarity, since MT minus-ends remain anchored to centrosomes. However, our simulations of spindle dynamics in the absence of Eg5 indicate that activity of spindle-pole-localized dynein, together with HSET, remains relevant as it functions to maintain close proximity of centrosomes following spindle pole collapse (Figure 4 B(i)). To next test that our model accurately reflects the known role of HSET activity in mitosis, we mimic HSET depletion by setting the binding probability to MTs (P_H) equal to zero. Published biological results show that spindle length increases with HSET inhibition or depletion in the absence of stable kinetochore attachments [14]. Consistent with this, bipolar spindle length in our simulations increase from 15 μm for the base case to 17 μm (Figure 4 A(ii),D). Analyses of force generating MTs over time reveal that increased spindle length in the absence of HSET activity is driven by Eg5 and cortical dynein (Figure 4 B(ii)).

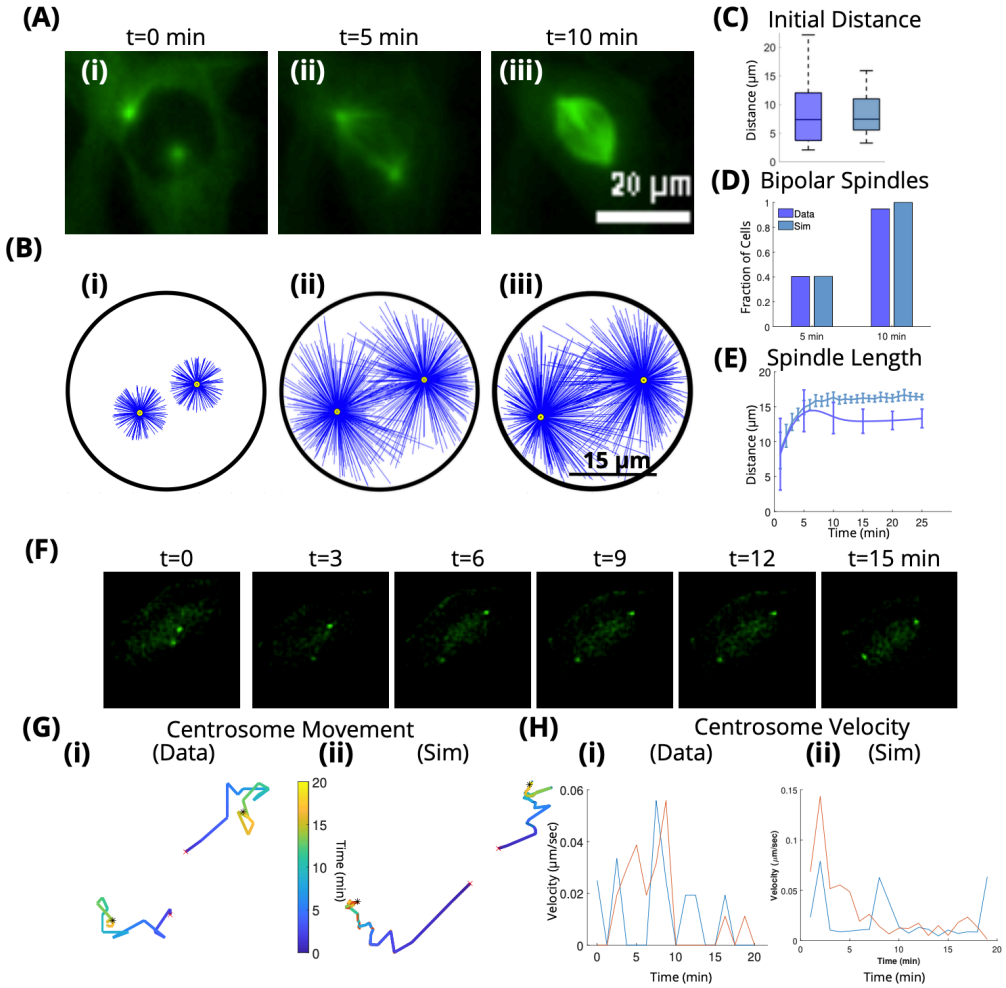

Figure 3: **Stochastic force-balance model captures centrosome movement and bipolar spindle formation.** (A) Still frames from live-cell imaging of RPE cells expressing EGFP-tubulin from the time point before nuclear envelope breakdown (NEB) at t=0 min in (i) to spindle bipolarity at t=10 min in (iii). (B) Still frames from a single simulation showing initial centrosome positioning at t=0 min in (i) to spindle bipolarity at t=10 min in (iii). (C) Distributions of initial distance between spindle poles from live-cell imaging (Data) and simulations (Sim). (D) Plot of the fraction of cells (Data) and simulations (Sim) that achieve bipolarity by 5 and 10 min. (E) Plot of the spindle length over time from live-cell imaging (Data) and simulations (Sim). Error bars are standard deviation. Biological data are captured at 5 min increments; a cubic spline is used to generate the curve. All averages for (C)-(E) calculated from at least 40 cells and 40 simulations. (F) Still frames from live-cell imaging of RPE cells expressing GFP-centrin. (G) (i) Experimental traces of centrosome movement from the movie shown in (F), where color denotes time (min). (G) (ii) Traces of centrosome movement from a single simulation, where the two lines correspond to the two centrosomes, and color denotes time (min). Red 'x' is initial centrosome position, black asterisk is final centrosome position. (H) (i) Centrosome velocities over time from movie shown in (F). (H) (ii) Centrosome velocities over time from simulation shown in (G)(ii). Each line is a centrosome.

Due to the dual function of dynein at spindle poles and the cell cortex, biological approaches have been unable to discern the specific role of cortical dynein in bipolar spindle formation. To address this limitation in our model, cortical dynein activity was depleted by setting the binding probability to MTs (P_d) to zero. Our simulations indicate that specific loss of cortical dynein results in shorter bipolar spindles, decreased from 15 μm in the base case to 10 μm. We additionally see a 2-fold increase in MTs bound to Eg5 and HSET when cortical dynein activity is absent compared to the base case (6% each from 3% each in the base case) (Figure 4 A(iii),B(iii),C,D).

Importantly, none of the single motor protein perturbations described have a significant impact on average MT length compared to the base condition (Figure 4 E). As such, the changes in bipolar spindle length following perturbations

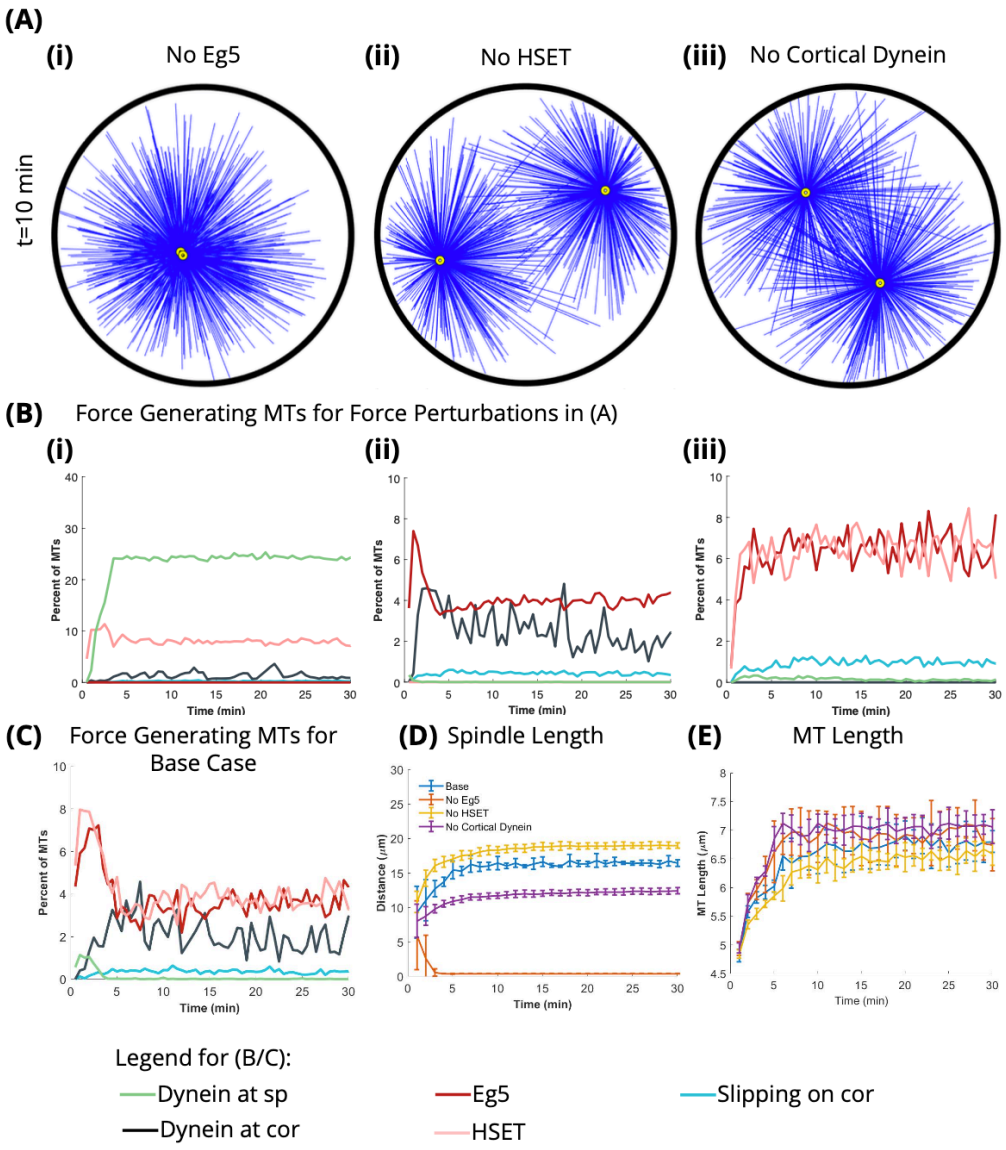

Figure 4: **Force perturbations impact spindle bipolarity.** (A) Still frame from a simulation at t=10 min with no MTs binding to: (i) Eg5, (ii) HSET, (iii) cortical dynein. (B) Plot of the average percent of MTs in each force-generating state over time with no MTs binding to (i) Eg5, (ii) HSET, (iii) cortical dynein, and (C) the base case. (D) Plot of the average distance between spindle poles over time for the base case and each single force perturbation. (E) Plot of the average length of MTs over time. All averages are of 10 simulations and error bars shown correspond to standard deviation.

to motor activity are strictly a result of altered forces on the centrosomes. Combined, these results indicate that our model both captures known changes in bipolar spindle length following loss of Eg5 or HSET, and reveals changes in steady-state spindle length following loss of cortical dynein.

3.4 Cortical dynein is a primary regulator of bipolar spindle length

The biophysical model used here to describe and explore the dynamics of bipolar spindle formation and maintenance has the benefit of discretely defined MTs, each of which can generate force depending on its length and position relative to other intracellular components (described further in Appendix A) (Figure 5 A). To explore how the magnitude and direction of forces change during spindle formation, we assessed each component of the force over time, with respect to $\vec{V}_{cent}$, the vector between centrosomes (Appendix A, Figure A2 A) (using the projection of the total forces in the

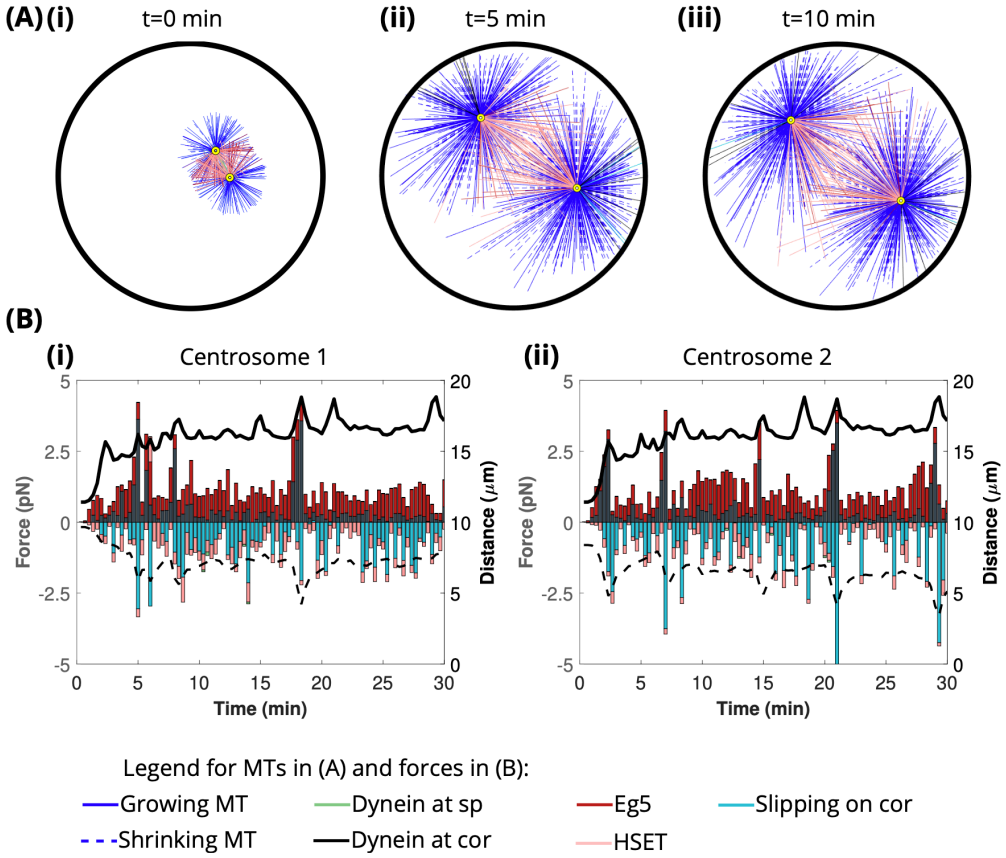

Figure 5: **Forces are dynamic over time, enabling the formation and maintenance of a bipolar spindle.** (A) Still frames from a simulation from initial centrosome positioning (i) to spindle bipolarity (iii). MT color represents its "state", defining the force that it generates. (B,C) Force plots of centrosome "1" and centrosome "2" in the direction of the vector between the two centrosomes, where a positive force brings centrosomes together and negative force pushes centrosomes apart. Black solid line shows spindle length over time and black dashed line shows the absolute minimum centrosome distance to the cell cortex over time.

direction of $\vec{V}_{cent}$). We considered a positive force to be one that increases spindle length (i.e. Eg5/cortical dynein) and a negative force to be one that decreases spindle length (i.e. HSET/pushing on the cell cortex/dynein at spindle poles).

To visualize how forces contribute to spindle dynamics, force plots for each centrosome were overlaid with curves for spindle length and the minimal centrosome distance to the cell cortex over time (Figure 5 B(i)-(ii)). In our base case, where we have no perturbed motor activity, we find dynamic and reproducible force-dependent changes in spindle dynamics. Our analysis reveals that Eg5 activity is high at early time points (t<5 min), indicating that early centrosome separation and bipolar spindle formation is driven by Eg5, consistent with the known biological role of Eg5 in mitosis [67, 68, 69]. Following early centrosome separation, spindle length reaches a quasi "steady-state". While averages over many simulations indicate that a stable spindle length is achieved (Figure 3 E), analysis of single simulations reveal oscillations in spindle length once a bipolar spindle has formed (Figure 5 B). Observing the force components on each centrosome reveals that peaks in cortical dynein coincide with both peaks in spindle length and valleys in the minimal centrosome distance to the cell cortex (Figure 5 B). This data suggests that MT binding to cortical dynein is responsible for changes in steady-state spindle length.

3.5 Cortical dynein drives oscillations in spindle length after spindle bipolarity is achieved

To confirm that changes in spindle length are a consequence of cortical dynein pulling forces, we reduced cortical dynein activity in the model by altering P_d, the probability of MTs binding to dynein at the cell cortex. This analysis reveals that as the dynein binding probability is decreased, bipolar spindle length decreases (16.5 μm when $P_d = 0.5$

to 14.6 μm when $P_d = 0.3$, and 12.6 μm $P_d = 0$) and the minimal centrosome distance to the cell cortex increases (Figure 6 A,D, Supplemental Figure S3).

To define a time-dependent relationship between cortical dynein binding and bipolar spindle length, we performed quantitative time-series analyses. The data is represented as a kymograph, a graphical representation of position over time, where the y-axis represents time (Figure 6 B). In each plot, $x = 0$ is the center of the cell and $x = -15$, $x = 15$ are the cell boundaries. Red asterisks indicate centrosome position at 20 sec time intervals. We used peak prominence [70], defined as the vertical distance between the height of a peak and its lowest contour line, as a readout of significant changes in spindle length, where peaks identified as significant had a prominence of at least 1 μm. As shown in Figure 6 B,D, oscillations in bipolar spindle length have both decreased frequency and amplitude when cortical dynein activity is decreased (when $P_d = 0.5$, 0.3, 0, the average number of prominent peaks=5, 1, 1 and peak width=35.5, 37.4, 38.7 s, respectively). To further characterize the relationship between cortical dynein binding and bipolar spindle length, we performed cross-correlation analysis [71]. Results indicate that cortical dynein binding and spindle length are highly correlated at a lag of 0 min, with an average correlation coefficient of 0.62, revealing that peaks in cortical dynein binding occurs simultaneously with significant changes in bipolar spindle length. Together, this data suggests that cortical dynein activity during mitosis is required for a *dynamic* bipolar spindle and is responsible for oscillations in steady-state spindle length.

3.6 Changes to interpolar forces, in the absence of cortical dynein, rescues spindle length but not spindle dynamics

To further define the relationship between MT-derived forces and the maintenance of spindle bipolarity in the presence or absence of cortical dynein, we decreased HSET binding and/or increased Eg5 binding. Individually, each perturbation in the absence of cortical dynein activity partially rescues bipolar spindle length; with the most extreme conditions ($P_H = 0$ or $P_E = 1$) achieving a final spindle length of 15.2 μm and 14.2 μm, respectively, compared to the base case (positive control) at 16.5 μm and 12.6 μm when only cortical dynein activity is perturbed (negative control) (Figure 7 A,C,E). A combination of HSET inhibition ($P_H = 0$) *and* maximum Eg5 activity ($P_E = 1$) is needed to fully restore bipolar spindle length (Figure 7 A,B). Nevertheless, perturbations to HSET or Eg5 activity alone, or in conjunction, is insufficient to rescue oscillations in pole-to-pole distance in the absence of cortical dynein, reaffirming the requirement of cortical dynein for changes in bipolar spindle length (Figure 7 C,E).

We performed the same perturbations to motor activity in the presence of cortical dynein to confirm that dynein activity is required for oscillations in bipolar spindle length. Here, these perturbations contribute to additive changes in spindle length, increasing from 16.5 μm in the base case to 19.9 μm in the most extreme condition ($P_H = 0$, $P_E = 1$) (Figure 7 B,E). Importantly, additional force perturbations to HSET or Eg5 activity do not impact oscillations in bipolar spindle length in the presence of cortical dynein, as the number of prominent peaks remains similar to that of the base case (Figure 7 D,E). Together this data suggests that while spindle length is sensitive to both HSET and/or Eg5, cortical dynein remains the dominant regulator of spindle length oscillations.

3.7 Cortical dynein is required for spindle bipolarity when HSET activity is high

HSET overexpression is prominent in many cancer contexts, where it is necessary to efficiently cluster supernumerary centrosomes [72, 73, 74, 75, 55, 76]. In addition, high HSET expression corresponds with increased cell proliferation independent of centrosome number, suggesting that HSET-dependent mitotic regulation may be relevant to cancer [77, 78]. To model high HSET activity, we incrementally increased the HSET binding probability from its base level of $P_H = 0.5$. Our simulations indicate that spindle bipolarity is sensitive to HSET activity, such that the incidence of spindle pole collapse increases with high HSET activity, with only 40% of simulations forming a bipolar spindle when $P_H = 0.9$ and 0% when $P_H = 1$ (Figure 8 A). To determine the force requirements for bipolar spindle formation in the presence of high HSET ($P_H = 0.9$), we explored a range of increasing cortical dynein activity and found that spindle bipolarity is rescued by cortical dynein activity in a concentration-dependent manner, with 80% of simulations forming a bipolar spindle when $P_d = 1$ (Figure 8 B).

Work from other groups indicates that HSET-dependent motor activity is a dominant force in centrosome clustering once centrosomes reach a critical distance of 7-8 μm from each other, whereas centrosome pairs are not impacted by HSET activity when they are 11-12 μm apart [79]. Consistent with this, we find that centrosomes collapse when they are, on average, initially 6.7 μm apart, and instead form a bipolar spindle when intial centrosome distance is, on average, 10.4 μm apart. Together, these results indicate that high cortical dynein activity and/or a large initial centrosome distance promotes bipolar spindle formation in the presence of high HSET.

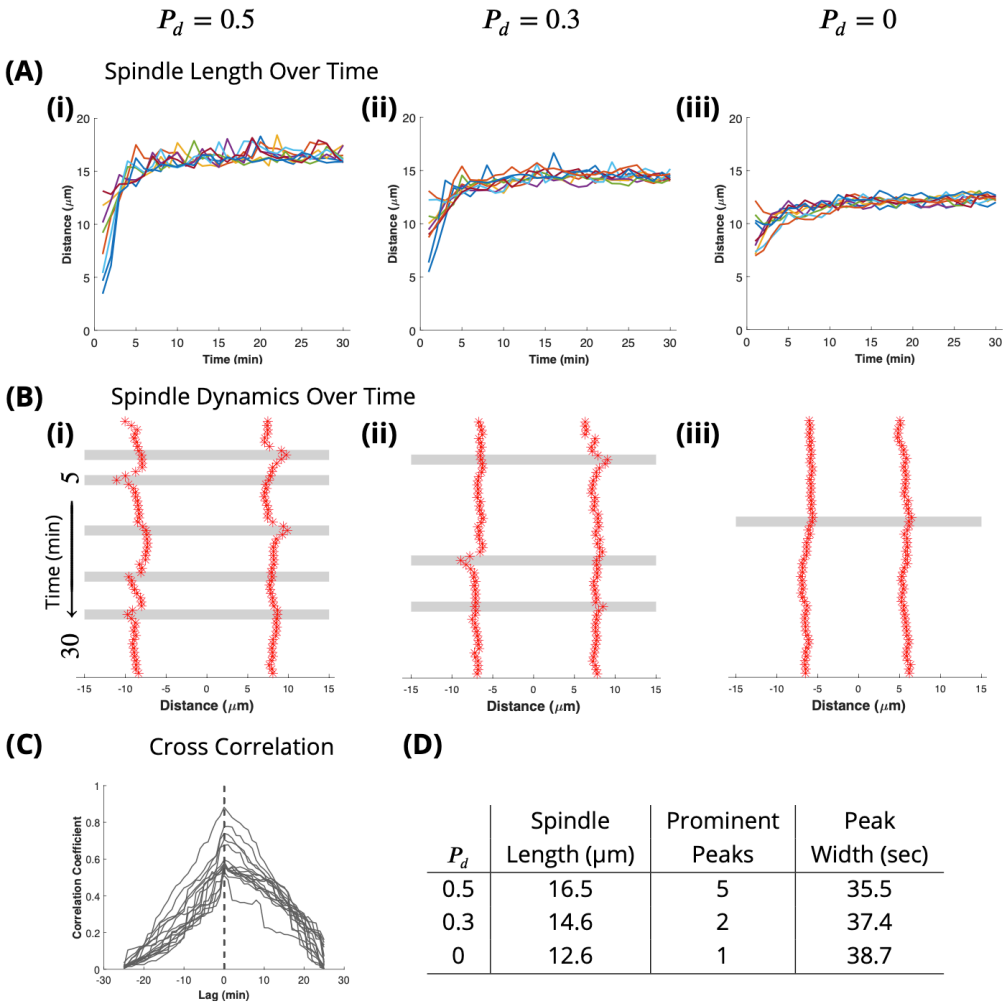

P_d	Spindle Length (μm)	Prominent Peaks	Peak Width (sec)
0.5	16.5	5	35.5
0.3	14.6	2	37.4
0	12.6	1	38.7

Figure 6: **Cortical dynein regulates spindle length and bipolar spindle dynamics.** (A) Curves of spindle length over time for 10 simulations with a dynein binding probability of 0.5 in (i), 0.3 in (ii), and 0 in (iii). (B) Representative kymograph of a single simulation with dynein binding probability 0.5 in (i), 0.3 in (ii), and 0 in (iii) from 5 to 30 minutes. Red asterisks are centrosome position plotted every 20 seconds, gray bars indicate prominent peaks in spindle length. (C) Cross correlation analysis of spindle length and cortical dynein binding. Each gray line is a centrosome, traces from 10 simulations are shown. Black vertical dashed line represents the average maximum correlation coefficient (at t=0 min). (D) Table showing average spindle length, number of prominent peaks, and width of prominent peaks from 10 simulations for each dynein binding probability.

4 Conclusions

The biophysical model presented here forms and maintains a bipolar mitotic spindle through the balance of five MT-derived forces, including MT interactions with three key motor proteins: HSET, Eg5, and dynein (Figures 1, 3, 5). Our model was based on and validated using our experimental data defining initial centrosome position and time-dependent changes in spindle bipolarity in mammalian cells (Figures 2, 3). Biological inhibition or knockdown of Eg5 or HSET are shown to alter spindle length [14, 9, 46, 47, 48], and disruption of Eg5 or HSET binding to MTs in our model closely reflects this, demonstrating that our biphysical model captures known biological phenomena (Figure 4).

The role of dynein activity in spindle formation has been difficult to discern because of its localization and function at both spindle poles and the cell cortex during mitosis [39, 41]. By defining these motor populations independently in our model, we sought to specifically define the role of cortical dynein activity in spindle bipolarity. Previous work has shown that the position, orientation, and oscillatory movement of the bipolar spindle is regulated, in part, by cortical dynein [43, 42, 44]. Results from our model further reveal that cortical dynein activity positively influences average

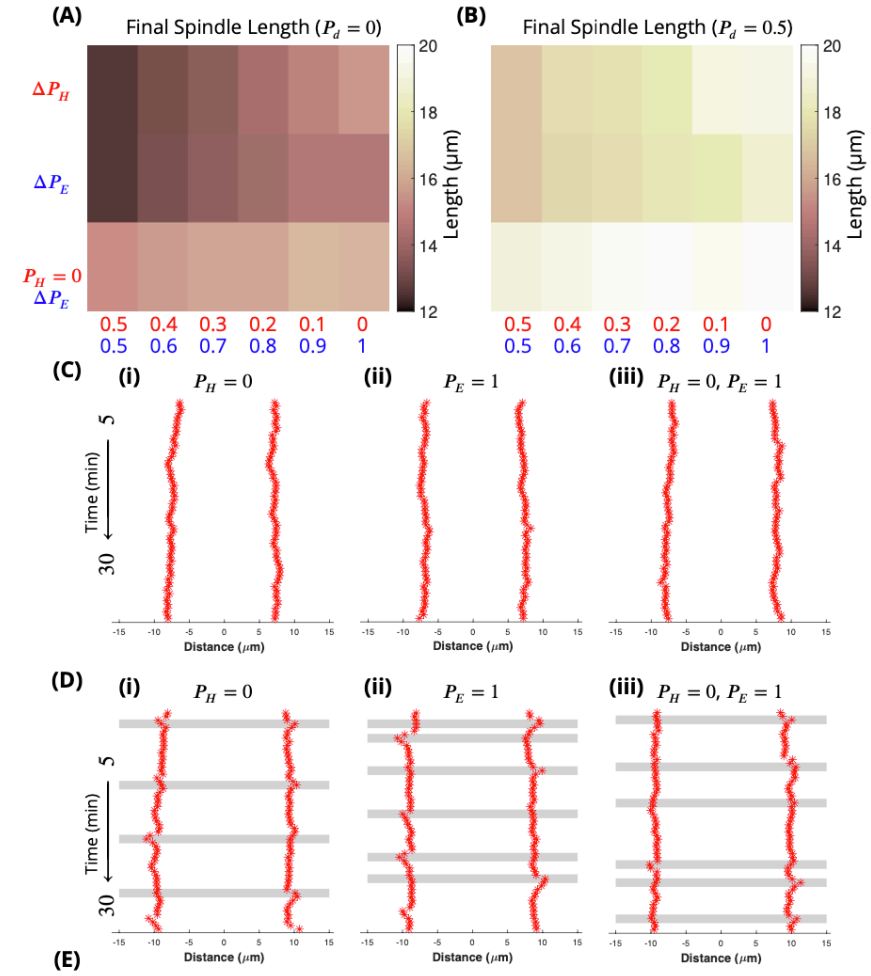

Condition	$P_d = 0.5$	$P_d = 0$	$P_d = 0$ $P_H = 0$	$P_d = 0$ $P_E = 1$	$P_d = 0$ $P_H = 0$ $P_E = 1$	$P_H = 0$	$P_E = 1$	$P_H = 0$ $P_E = 1$
Spindle Length (μm)	16.5	12.6	14.2	15.2	16.1	19.2	18.7	19.9
Prominent Peaks	5	1	1	1	1	4	4	5
Peak Width (sec)	35.5	38.7	43.6	35.5	36.4	31.3	35.2	31.7

Figure 7: **Additional force perturbations rescue spindle length, but not spindle dynamics, in the absence of cortical dynein.** (A,B) Heat maps showing the average final spindle length under varied conditions, in the absence (A) or presence (B) of cortical dynein. ΔP_H and ΔP_E represent the changes in HSET and/or Eg5 binding probabilities, respectively, where the probabilities are shown below the heatmap in red (ΔP_H) and blue (ΔP_H).(C) Representative kymographs of varied Eg5/HSET binding probabilities, in the absence (C) or presence (D) of cortical dynein. Gray bars indicate prominent peaks in spindle length, kymographs in (C) have no prominent peaks. (E) Table of average final spindle length, average number of prominent peaks, and average peak width under different conditions. All data averaged over 10 simulations for each condition.

spindle length and promotes oscillations in pole-to-pole distance over time (Figure 4, 6). While decreased bipolar spindle length in the absence of cortical dynein can be rescued by additional force perturbations to HSET and/or Eg5 activity, dampened spindle length oscillations are not restored, suggesting that cortical dynein is essential for this behavior (Figure 7). Additionally, we find that high cortical dynein activity is required for bipolar spindle formation

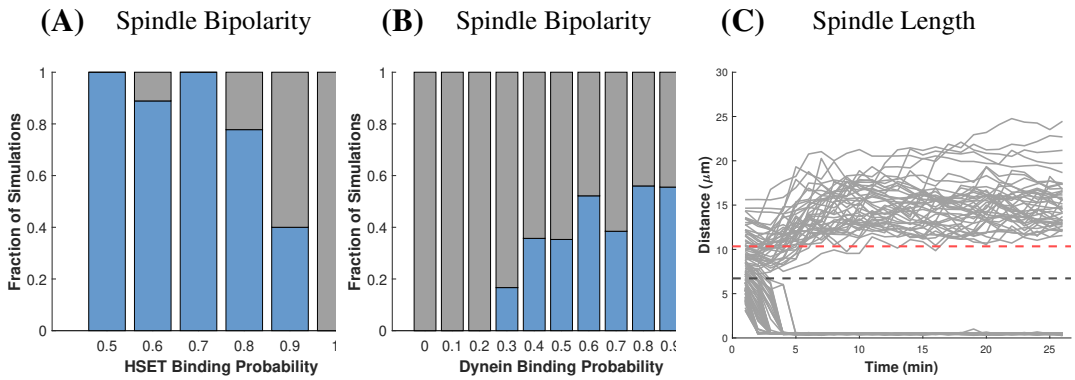

Figure 8: **High cortical dynein promotes spindle bipolarity in the presence of high HSET.** (A) Fraction of simulations that form a bipolar spindle with varying levels of HSET. (B) Fraction of simulations that form a bipolar spindle in the presence of high HSET ($P_{HSET} = 0.9$) with varying levels of cortical dynein. (C) Plots of spindle length over time of simulations with high HSET ($P_{HSET} = 0.9$) and varying levels of cortical dynein that have simulations that form a bipolar spindle ($0.2 < P_d \leq 1$). Red dashed line is the average initial distance of centrosomes that separate (10.4 μm) and black dashed line is the average initial distance of centrosomes that collapse (6.7 μm). Data from 20 simulations for each condition.

when HSET activity is also high (Figure 8), as has been described in some cancer contexts [77, 78]. Overall, we provide a mathematical and computational framework to inform future studies and explore the contributions of individual force components on centrosome movement, spindle dynamics, and centrosome clustering.

5 Acknowledgments

Results in this paper were obtained in part using a high-performance computing system acquired through NSF MRI grant DMS-1227943 to WPI. We thank Neil Ganem for supplying RPE GFP-Centrin cell line and the members of the Manning lab for feedback throughout the writing process. ALM is supported by a Smith Family Award for Excellence in Biomedical Research and DLM is supported by a NSF-GRFP.

References

[1] E.H. Hinchliffe. The centrosome and bipolar spindle assembly. Cell Cycle, 10:3841–3848, 2011.

[2] M.W. Kirschner and T. Mitchison. Microtubule dynamics. Nature, 324:621, 1986.

[3] M.M. Mogensen, A. Malik, M. Piel, V. Bouckson-Castaing, and M. Bornens. Microtubule minus-end anchorage at centrosomal and non-centrosomal sites: the role of ninein. J. Cell Sci., 113:3013–3023, 2000.

[4] M.K. Gardner, M. Zanic, C. Gell, V. Bormuth, and J. Howard. Depolymerizing kinesins Kip3 and MCAK shape cellular microtubule architecture by differential control of catastrophe. Cell, 147:1092–1103, 2011.

[5] M.K. Gardner, M. Zanic, and J. Howard. Microtubule catastrophe and rescue. Curr. Opinion Cell Biol., 25:14–22, 2013.

[6] C.L. Hueschen, S.J. Kenny, K. Xu, and S. Dumont. NuMA recruits dynein activity to microtubule minus-ends at mitosis. eLife, 6:1–26, 2017.

[7] S. Dumont and T.J. Mitchison. Force and length in the mitotic spindle. Curr. Biol., 19:R749–R761, 2009.

[8] Z.Y. She and W.X. Yang. Molecular mechanisms of kinesin-14 motors in spindle assembly and chromosome segregation. J. Cell Sci., 130:2097–2110, 2017.

[9] B.J. Mann and P. Wadsworth. Kinesin-5 regulation and function in mitosis. Trends Cell Biol., 29:66–79, 2019.

[10] R.G.H.P. van Heesbeen, M.E. Tanenbaum, and R.H. Medema. Balanced activity of three mitotic motors is required for bipolar spindle assembly and chromosome segregation. Cell Rep., 8:948–956, 2014.

[11] J. Zhou, J. Yao, and H.C. Joshi. Attachment and tension in the spindle assembly checkpoint. J. Cell Sci., 115:3547–3555, 2002.

[12] J.G. DeLuca, B. Moree, J.M. Hickey, J.V. Kilmartin, and E.D. Salmon. hnuf2 inhibition blocks stable kinetochore-microtubule attachment and induces mitotic cell death in HeLa cells. J. Cell Biol., 159:549–555, 2002.

[13] A.L. Manning and D.A. Compton. Mechanisms of spindle-pole organization are influenced by kinetochore activity in mammalian cells. Curr. Biol., 17:260–265, 2007.

[14] S. Cai, L.N. Weaver, S.C. Ems-McClung, and C.E. Walczak. Kinesin-14 family proteins hset/xtck2 control spindle length by cross-linking and sliding microtubules. Mol Biol Cell, 20:1348–1359, 2009.

[15] H.Y. Wu, E. Nazockdast, M.J. Shelley, and D.J. Needleman. Forces positioning the mitotic spindle: theories, and now experiments. Bioessays, 9:1600212, 2016.

[16] W.E. Channels, F.J. Nedelec, Y. Zheng, and PA. Iglesias. Spatial regulation improves antiparallel microtubule overlap during mitotic spindle assembly. Biophys. J., 94:2598–2609, 2008.

[17] E.N. Cytrynbaum, J.M. Scholey, and A.M. Mogilner. A force balance model of early spindle pole separation in drosophila embryos. Biophys. J., 84:757–769, 2003.

[18] C. Edelmaier, A.R. Lamson, Z.R. Gergley, S. Ansari, R. Blackwell, J.R. McIntosh, M.A. Glaser, and M.D. Betterton. Mechanisms of chromosome biorientation and bipolar spindle assembly analyzed by computational modeling. eLife, 9:e48787, 2020.

[19] M.E. Janson, R. Loughlin, I. Loiodice, C. Fu, D. Brunner, and F. Nedelec. Crosslinkers and motors organize dynamic microtubules to form stable bipolar arrays in fission yeast. Cell, 128:357–368, 2007.

[20] A.R. Lamson, C.J. Edelmaier, M.A. Glaser, and M.D. Betterton. Theory of cytoskeletal reorganization during cross-linker-mediated mitotic spindle assembly. Biophys. J., 116:1719–1731, 2019.

[21] J. Li and H. Jiang. Regulating positioning and orientation of mitotic spindles via cell size and shape. Phys. Rev. E, 97:012407, 2018.

[22] R. Loughlin, R. Heald, and F. Nedelec. A computational model predicts xenopus meiotic spindle organization. J. Cell Biol., 191:1239–1249, 2010.

[23] S. Sutradhar, S. Basu, and R. Paul. Intercentrosomal angular separation during mitosis plays a crucial role for maintaining spindle stability. Phys. Rev. E, 92:042714, 2015.

[24] E.J. Banigan, K.K. Chiou, E.R. Ballister, A.M. Mayo, M.A. Lampson, and A.J. Liu. Minimal model for collective kinetochore-microtubule dynamics. Proc. Natl. Acad. Sci. U.S.A., 112:12699–12704, 2015.

[25] O. Campas and P. Sens. Chromosome oscillation in mitosis. Phys. Rev. Lett., 97:128102, 2006.

[26] G. Civelekoglu-Scholey, D.J. Sharp, A. Mogilner, and J.M. Scholey. Model of chromosome motility in Drosophila embryos: adaptation of a general mechanism for rapid mitosis. Biophys. J., 90:3966–3982, 2006.

[27] A. Dinarina, C. Pugieux, M.M. Corral, M. Loose, J. Spatz, E. Karsenti, and F. Nedelec. Chromatin shapes the mitotic spindle. Cell, 138:502–513, 2009.

[28] V. Magidson, R. Paul, N. Yang, J.G. Ault, C.B. O'Connell, I. Tikhonenko, B.F. McEwen, A. Mogilner, and A. Khodjakov. Adaptive changes in the kinetochore architecture facilitate proper spindle assembly. Nat. Cell Biol., 17:1134–1144, 2015.

[29] R. Wollman, E.N. Cytrynbaum, J.T. Jones, T. Meyer, J.M. Scholey, and A. Mogilner. Efficient chromosome capture requires a bias in the 'search-and-capture' process during mitotic-spindle assembly. Curr. Biol., 15:828–832, 2005.

[30] I. Brust-Mascher, G. Civelekoglu-Scholey, M. Kwon, A. Mogilner, and J.M. Scholey. Model for anaphase B: role of three mitotic motors in a switch from poleward flux to spindle elongation. Proc. Natl. Acad. Sci. U.S.A., 101:15938–15943, 2004.

[31] C. Kozlowski, M. Srayko, and F. Nedelec. Cortical microtubule contacts position the spindle in c. elegans embryo. Cell, 129:499–510, 2007.

[32] J.J. Ward, H. Roque, C. Antony, and F. Nedelec. Mechanical design principles of a mitotic spindle. eLife, 3:e03398, 2014.

[33] L. Laan, N. Pavin, J. Husson, G. Romeg-Lemonne, M. van Duijn, M.P. Lopez, R.D. Vale, F. Julicher, S.L. Reck-Peterson, and M. Dogterom. Cortical dynein controls microtubule dynamics to generate pulling forces that reliably position microtubule asters. Cell, 148:502–514, 2012.

[34] L. Laan, S. Roth, and M. Dogterom. End-on microtubule-dynein interactions and pulling-based positioning of microtubule organizing centers. Cell Cycle, 11:3750–3757, 2012.

[35] M. Biro, Y. Romeo, S. Kroschwald, M. Bovellan, A. Boden, J. Tcherkezian, P.P. Roux, G. Charras, and E.K. Paluch. Cell cortex composition and homeostasis resolved by integrating proteomics and quantitative imaging. Cytoskeleton, 70:741–754, 2013.

[36] O.M. Lancaster, M. Le Berre, A. Dimitracopoulos, D. Bonazzi, E. Zlotek-Zlotkiewicz, R. Picone, T. Duke, M. Piel, and B. Baum. Mitotic rounding alters cell geometry to ensure efficient bipolar spindle formation. Dev. Cell, 25:270–283, 2013.

[37] P. Kunda, A.E. Pelling, T. Liu, and B. Baum. Moesin controls cortical rigidity, cell rounding, and spindle morphogensis during mitosis. Curr. Biol., 18:91–101, 2008.

[38] R. Tan, P.J. Foster, D.J. Needleman, and R.J. McKenny. Cooperative accumulation of dynein-dynactin at microtubule minus-ends drives microtubule network organization. Dev. Cell, 44:233–247, 2018.

[39] J. Gaetz and T.M. Kapoor. Dynein/dynactin regulate metaphase spindle length by targeting depolymerizing activities to spindle poles. J. Cell Biol., 166:465–471, 2004.

[40] V. Mountain, C. Simerly, L. Howard, A. Ando, G. Schatten, and D. A. Compton. The kinesin-related protein, Hset, opposes the activity of Eg5 and cross-links microtubules in the mammalian mitotic spindle. J. Cell Biol., 147:351, 1999.

[41] G. Goshima, F. Nedelec, and R.D. Vale. Mechanisms for focusing mitotic spindle poles by minus end-directed motor proteins. J. Cell Biol., 171:220, 2005.

[42] T. Kiyomitsu and I.M. Cheeseman. Chromosome-and spindle-pole derived signals generate an intrinsic code for spindle position and orientation. Nat. Cell Biol., 14:311–317, 2012.

[43] S. Kotak, C. Busso, and P.J. Gonczy. Cortical dynein is critical for proper spindle positioning in human cells. Cell Biol., 199:97–110, 2012.

[44] M. Okumura, T. Natsume, M.T. Kanemaki, and T. Kiyomitsu. Dynein-dynactin-NuMA clusters generate cortical spindle-pulling forces as a multi-arm ensemble. eLife, 7:e36559, 2018.

[45] J. Wu, G. Misra, R.J. Russell, A.J. Ladd, T.P. Lele, and R.B. Dickinson. Effects of dynein on microtubule mechanics and centrosome positioning. Mol. Biol. Cell, 22:4834–4841, 2011.

[46] D.J. Sharp, G.C. Rogers, and J.M. Scholey. Microtubule motors in mitosis. Nature, 407:41–47, 2000.

[47] T.M. Kapoor, T.U. Mayer, M.L. Coughlin, and T.J. Mitchison. Probing spindle assembly mechanisms with. moastrol, a small molecule inhibitor of the mitotic kinesin, Eg5. J. Cell Biol., 150:975–988, 2000.

[48] T.U. Mayer, T.M. Kapoor, S.J. Haggarty, R.W. King, S.L. Schreiber, and T.J. Mitchison. Small molecule inhibitor of mitotic spindle bipolarity identified in a phenotype-based screen. Science, 286:971–974, 1999.

[49] G.Y. Chen, Y.J. Kang, S.A. Gayek, W. Youyen, E. Tuzel, R. Ohi, and W.O. Hancock. Eg5 inhibitors have contrasting effect on microtubule stability and metaphase spindle integrity. ACS Chem. Biol., 12:1038–1046, 2017.

[50] A. Burakov, E. Nadezhdina, B. Slepchenko, and V. Rodinov. Centrosome positioning in interphase cells. J. Cell Biol., 162:963–969, 2003.

[51] K. Luby-Phelps, S. Mujumdar, R.B. Mujumdar, L.A Ernst, W. Galbraith, and A.S. Waggoner. A novel fluorescence ratiometric method confirms the low solvent viscosity of the cytoplasm. Biophys. J., 65:236–242, 1993.

[52] R.R. Wei, P.K. Sorger, and S.C. Harrison. Molecular organization of the ndc80 complex, and essential kinetochore component. Proc Natl Acad Sci USA, 102:5363–5367, 2005.

[53] T. Hori, T. Haraguchi, Y. Hiraoka, H. kimura, and T. Fukagawa. Dynamic behavior of nuf2-hec1 complex that localizes to the centrosome and centromere and is essential for mitotic progression in mitotic cells. J Cell Sci., 116:3347–3362, 2003.

[54] D.L. Mercadante and A.L. Crowley, E.A. amd Manning. Live cell imaging to assess the dynamics of metaphase timing and cell fate following mitotic spindle perturbations. J. Vis. Exp, 151, 2019.

[55] N.J. Ganem, S.A. Godinho, and D. Pellman. A mechanism linking extra centrosomes to chromosomal instability. Nature, 460:278–282, 2009.

[56] M. Piehl and L. Cassimeris. Organization and dynamics of growing microtubule plus ends during early mitosis. Mol. Biol. Cell, 14:916–925, 2003.

[57] T.J. Mitchison. Polewards microtubule flux in the mitotic spindle: evidence from photoactivation of fluorescence. J. Cell Biol., 109:637–642, 1989.

[58] Y.A. Komarova, A.S. Akhmanova, S. Kojima, N. Galjart, and G.G. Borisy. Cytoplasmic linker proteins promote microtubule rescue in vivo. J. Cell Biol., 159:589–599, 2002.

[59] R. Ma, L. Laan, M. Dogterom, N. Pavin, and F. Julicher. General theory for the mechanics of confined microtubule asters. New J. Phys., 16:013018, 2013.

[60] M. Piehl, U.S. Tulu, P. Wadsworth, and L. Cassimeris. Centrosome maturation: measurement of microtubule nucleation throughout the cell cycle by using GFP-tagged EB1. Proc. Natl. Acad. Sci. U.S.A., 101:1584–1588, 2004.

[61] M.M. Elshenawy, J.T. Canty, L. Oster, L.S. Ferro, Z. Zhou, S.C. Blanchard, and A. Yildiz. Cargo adaptors regulate stepping and force generation of mammalian dynein-dynactin. Nat Chem Biol, 15:1093–1101, 2019.

[62] L. Urnavicius, C.K. Lau, M.M. Elshenawy, E. Morales-Rios, C. Motz, A. Yildiz, and A.P. Carter. Cryo-em shows how dynactin recruits two dyneins for faster movement. Nature, 554:202–206, 2018.

[63] Y. Shimamoto, S. Forth, and T.M. Kapoor. Measuring pushing and braking forces generated by ensembles of kinesin-5 crosslinking two microtubules. Dev. Cell, 34:669–681, 2015.

[64] J. Li, L. Cheng, and H. Jiang. Cell shape and intercellular adhesion regulate mitotic spindle orientation. Mol Biol Cell, 30, 2019.

[65] J. Roostalu, J. Rickman, C. Thomas, F. Nedelec, and T. Surrey. Determinants of polar versus nematic organization in networks of dynamic microtubules and mitotic motors. Cell, 175:796–808, 2018.

[66] S.A. Endow, R. Chandra, D.J. Komma, A.H. Yamamoto, and E.D. Salmon. Mutants of the drosophila ncd microtubule motor protein cause centrosomal and spindle pole defects in mitosis. J. Cell Sci., 107:859–867, 1994.

[67] A.S. Kashina, R.J. Baskin, D.G. Cole, K.P. Wedaman, W.M. Saxton, and J.M. Scholey. A bipolar kinesin. Nature, 379:270–272, 2009.

[68] L.C. Kapitein, E.J. Peterman, B.H. Kwok, J.H. Kim, T.M. Kapoor, and C.F. Schmidt. A bipolar mitotic kinesin moves on both microtubules that it crosslinks. Nature, 435:114–118, 2005.

[69] M.E. Tanenbaum and R.H. Medema. Mechanisms of centrosome separation and bipolar spindle assembly. Dev. Cell, 19:797–806, 2010.

[70] MathWorks. findpeaks, 2007.

[71] MathWorks. xcorr, 2009.

[72] J.Y. Chan. A clinical overview of centrosome amplification in human cancers. Int. J. Biol. Sci., 7:1122–1144, 2011.

[73] J. Kwon, S. Godinho, N.S. Chandhok, N.J. Ganem, A. Azioune, M. Thery, and D. Pellman. Mechanisms to suppress multipolar divisions in cancer cells with extra centrosomes. Genes Dev., 22:2189–2203, 2019.

[74] B. Navarro-Serer, E.P. Childers, N.M. Hermance, D. Mercadante, and A.L. Manning. Aurora A inhibition limits centrosome clustering and promotes mitotic catastrophe in cells with supernumerary centrosomes. Oncotarget, 10:1649–1659, 2019.

[75] N.J. Quintyne, J.E. Reing, D.R. Hoffelder, S.M. Gollin, and W.S. Saunders. Spindle multipolarity is prevented by centrosomal clustering. Science, 307:127–129, 2005.

[76] F. Galimberti, S.L. Thompson, S. Ravi, D.A. Compton, and E. Dmitrovsky. Anaphase catastrophe is a target for cancer therapy. Clin. Cancer Res., 17:1218–1211, 2011.

[77] V. Pannu, P. Rida, A. Ogden, R. Turaga, S. Donthamsetty, N. Bowen, K. Rudd, M. Gupta, M. Reid, G. Cantauria, C. Walczak, and R. Aneja. Hset overexpression fuels tumor progression via centrosome clustering-independent mechanisms in breast cancer patients. Oncotarget, 6:6079–6091, 2015.

[78] J. Klaylein-Sohn, B. Pollinger, M. Ohmer, F. Hofmann, E. Nigg, B. Hemmings, and M. Wartmann. Acentrosomal spindle organization renders cancer cells dependent on the kinesin hset. J. Cell Sci., 125:5391–5402, 2012.

[79] A.D. Rhys, P. Monteiro, C. Smith, M. Vaghela, T. Arnandis, T. Kato, B. Leitinger, E. Sahai, A. McAinsh, G. Charras, and S.A. Godinho. Loss of E-cadherin provides tolerance to centrosome amplification in epithelial cancer cells. J. Cell Biol., 217(1):195–209, 2018.

[80] C.E. Walczak, I. Vernos, T.J. Mitchison, E. Karsenti, and R. Heald. A model for the proposed roles of different microtubule-based motor proteins in establishing spindle bipolarity. Curr. Biol., 8:903–913, 1998.

[81] F. Decker, D. Oriola, B. Dalton, and J. Bruges. Autocatalytic microtubule nucleation determines the size and mass of xenopus laevis egg extract spindle. eLife, 7:e31149, 2018.

[82] K. Svoboda and S.M. Block. Force and velocity measured for single kinesin molecules. Cell, 77:773–784, 1994.

[83] S. Chatterjee, A. Sarker, A. Khodjakov, A. Mogilner, and R. Paul. Mechanics of multi-centrosomal clustering in bipolar mitotic spindles. In Press, preprint at bioRxiv 0.1101/2019.12.17.879817, 2020.

6 Supplementary Material

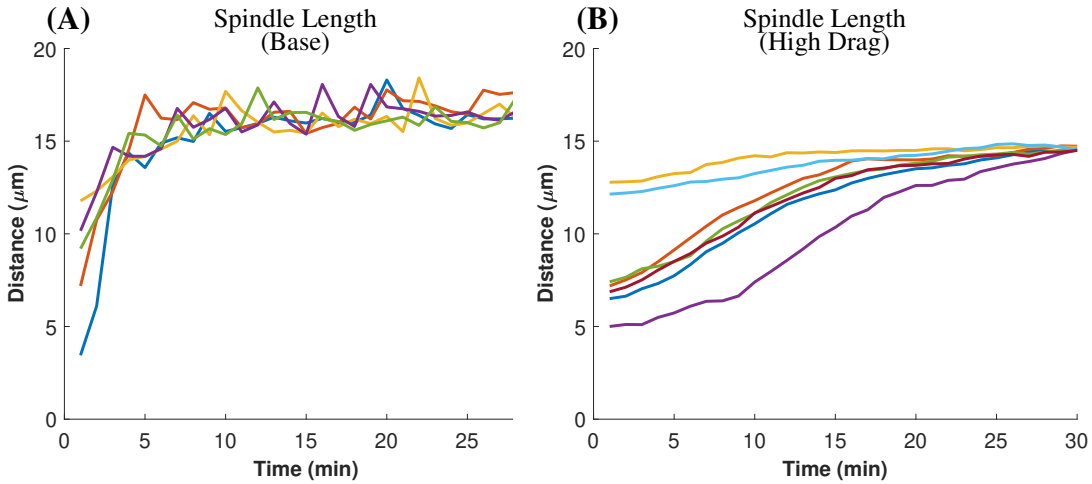

Figure S1: **Increasing the drag coefficient alters the dynamics of bipolar spindle formation.** Curves of spindle length over time for the base case (A) and the high drag case (B). High drag is defined as 5ξ. Individual traces are shown for 6 simulations.

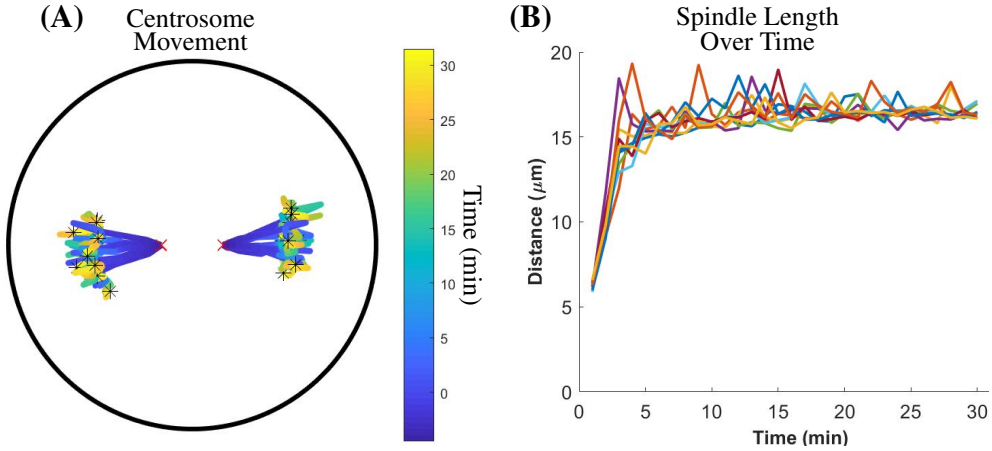

Figure S2: **Multiple simulations with the same initial centrosome positioning reveal variations due to model stochasticity.** (A) Centrosome movement traces over time for 10 simulations with the same initial centrosome positions. Red 'x' is initial position, black asterisk is final position. (B) Traces of spindle length over time for 10 simulations with the same initial centrosome positions. Each line is a simulation.

A Model Details

A.1 Microtubules

MTs are dynamic filaments that make up the mitotic spindle, which we model as elastic rods with a defined bending rigidity κ and buckling force f_{stall}. Initial MT angle α is chosen from a uniform distribution, $\alpha \in \mathcal{U}[0, 2\pi)$, around the circumference of the centrosome. We consider MT minus-ends to remain embedded in the centrosome, to account for

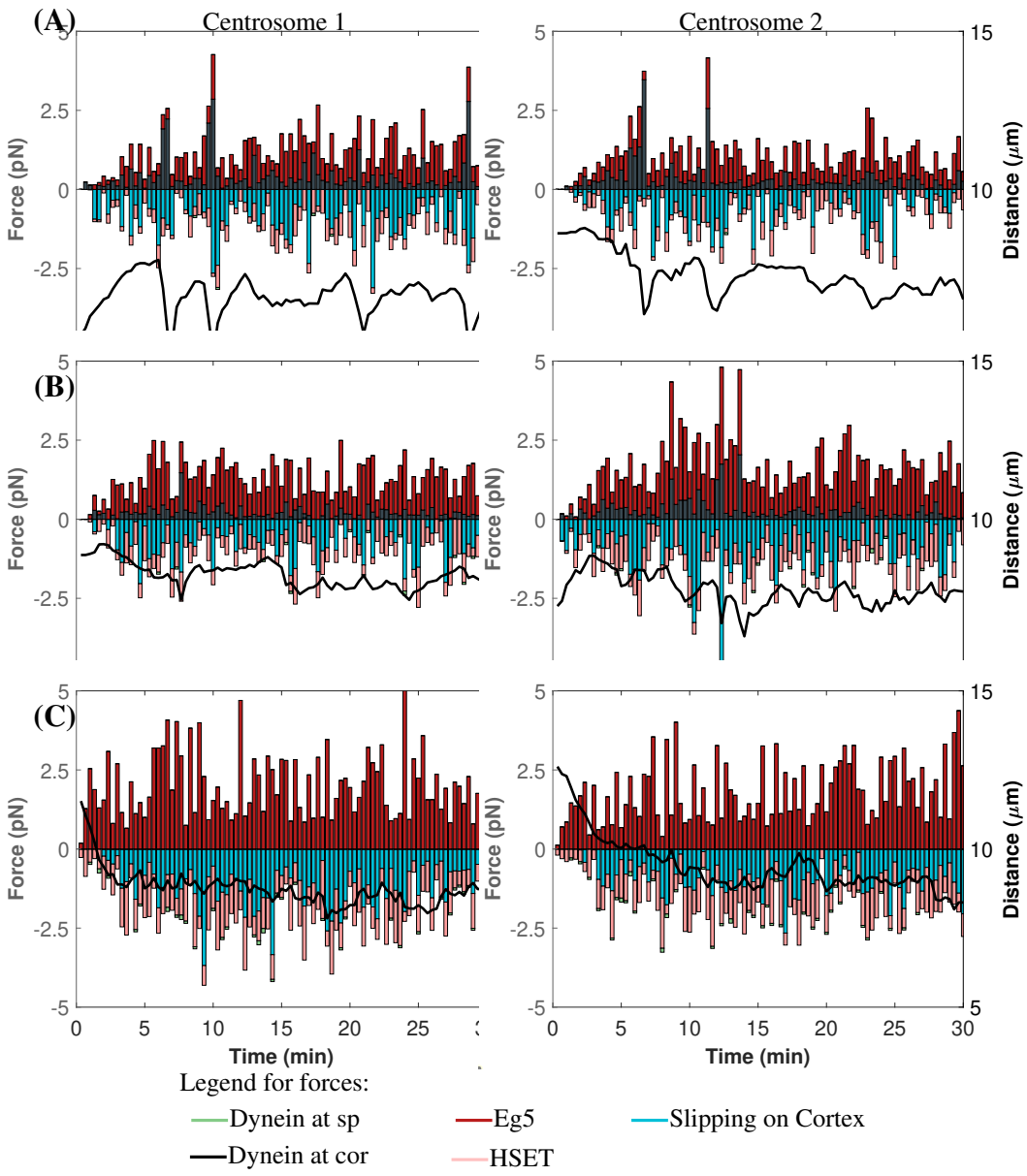

Figure S3: **Reduction and loss of cortical dynein impacts centrosome distance to the cell cortex.** Representative images of force components over time for a single simulation with $P_d = 0.5$ (A), $P_d = 0.3$ (B), $P_d = 0$ (C), overlaid with the minimal centrosome distance to the cell cortex (black line). A positive force is one that pushes centrosomes apart while a negative force is one that pulls centrosomes together. The left column is centrosome "1" and the right column is centrosome "2" from the same simulation.

crosslinkers that maintain spindle-pole focusing throughout mitosis [41, 80]. MT plus-ends undergo dynamic instability [2], meaning that they are stochastically switching between states of growing (at a velocity v_g) and shrinking (at a velocity v_s). MTs undergo rescue (switch from shrinking to growing) at a rate k_1 and undergo catastrophe (switch from growing to shrinking) at a MT-length dependent rate k_2, defined as $k_{2_i} = sv_g\ell_i$, where s is a scaling factor, ℓ_i is the length of the i^{th} MT, and dt is the time step [5]. Following a standard Monte Carlo method, we choose $n_2 \in \mathcal{U}[0, 1]$ and the i^{th} growing MT undergoes catastrophe if $n_2 \leq k_2^*$, where $k_2^* = 1 - e^{-k_{2_i}dt}$ [21]. Similarly, shrinking MT i will be rescued if $n_1 \leq k_1^*$ where $k_1^* = 1 - e^{-k_1 dt}$. MTs that fail to undergo rescue depolymerize completely and are no longer considered in the system when $\ell_i \leq v_g dt$. Nucleation of MTs occurs at a rate MT_{nuc} and is then prevented once MTs exceed a total length of M, accounting for limited tubulin in the system (Figure A1) [81].

A.2 Cortical Forces

We assume that MTs can either be pulled towards the cell cortex by binding to dynein or push and slip against the cell cortex when binding does not occur. Cortical dynein is assumed to be uniformly distributed along the boundary and each MT has a determined probability of binding and experiencing a dynein-based pulling force. If the end of a MT is within a distance $\mathcal{D}_{d_{cor}}$ to the boundary, binding to dynein will occur if $n_d \in \mathcal{U}[0,1]$ is less than the probability of binding to dynein, P_d. The force generated by cortical dynein on the i^{th} MT nucleated from the c^{th} centrosome follows a standard linear force-velocity relationship [82]:

$$f_i^{d_{cor}} = f_{0,d}\left(1 - \frac{v_{i,d}}{v_{0,d}}\right), \tag{2}$$

where $f_{0,d}$ is the stall force of dynein, $v_{0,d}$ is the walking velocity of dynein, and $v_{i,d}$ is defined as the difference between the magnitude of the centrosome velocity and the poleward flux (v_f) of the MT. The total pulling force by cortical dynein on the c^{th} centrosome is then:

$$\vec{F}_c = \sum_{i=1}^{N_{c,d_{cor}}} -f_i^{d_{cor}} \exp\left(-\frac{\ell_i}{K d_{cor}}\right)\vec{m}_i, \tag{3}$$

where $N_{c,d}$ is the total number of MTs on centrosome c that bind to cortical dynein, ℓ_i is the length of the MT, K is a scaling factor, $\vec{m}_i$ is a unit vector in the direction of the MT, and d_{cor} is the minimum distance from the centrosome to the cell cortex. Based on the sign conventions, $\vec{F}_c$ is calculated with $-f_i$ as the centrosome is being pulled towards the cortex in response to this force. Due to the exponential length scaling, the force acting on the centrosome from a MT bound to dynein decreases exponentially [83], and we use this for every MT-motor interaction considered in this model. MTs will stay bound to cortical dynein until the end of the MT is greater than a distance $\mathcal{D}_{d_{cor}}$ from the cell cortex, at which time it begins depolymerizing.

Alternatively, if the random number, n_d, is greater than the probability of binding to dynein, P_d, the MT instead slips along the boundary and experiences a pushing force. The pushing force is described as:

$$f_i^{slip} = min\left(f_{stall}, \frac{\pi^2\kappa}{\ell_i^2}\right), \tag{4}$$

where f_{stall} is the stall force of a MT and κ is the bending rigidity of the MT. This force is also dependent on MT length, ℓ_i, such that longer MTs are more likely to buckle than shorter MTs. The pushing force felt back on the c^{th} centrosome by the $N_{c,slip}$ MTs is then:

$$\vec{F}_c^{slip} = \sum_{i=1}^{N_{c,slip}} f_i^{slip}\vec{m}_i. \tag{5}$$

MTs that push against the cell cortex also experience a slight angle change $\delta = \theta\eta$, where η is randomly chosen as -1 or 1 to determine the direction of the angle change and θ is a parameter that determines the amount of angle change. The unit vector $\vec{m}_i$ in the direction of MT i is then updated by δ. A MT will stop pushing against the cell cortex if the end of the MT is greater than a distance $\mathcal{D}_{d_{cor}}$ from the cell cortex. Alternatively, if $n_d \leq P_d$ and the end of the MT is within $\mathcal{D}_{d_{cor}}$ from the cell cortex, a pushing MT can then bind to cortical dynein.

A.3 Interpolar Forces

Interpolar MTs, those having an angle within that of the slope between the two centrosomes and the line perpendicular to the slope (Figure A2 A), can experience pushing or pulling forces by being bound to opposing MTs by either Eg5 or HSET, respectively. We discretize each MT to determine the proximity to other MTs. If MTs i, j nucleated from centrosomes c, k, respectively, are within a distance $\mathcal{D}_{Eg5,HSET}$ from each other, we then calculate the probability of binding to either Eg5 or HSET using a similar Monte Carlo Method as described previously; if a random number n_{Eg5}, n_{HSET} is less than P_E, P_H, binding of Eg5 or HSET occurs, respectively. A MT cannot be bound to both Eg5 and HSET.

The force on each MT by either Eg5 or HSET follows Equation (2) with stall forces $f_{0,Eg5}$, $f_{0,HSET}$ and walking velocities $v_{0,Eg5}$, $v_{0,HSET}$, respectively. Recall that these motors act at MT overlap regions in opposite directions. So,

while the stall force of HSET is positive in the force-velocity relationship, the force of Eg5 is negative. The total force by MTs bound to Eg5 or HSET on centrosome c is:

$$\vec{F}_c^{Eg5} = \sum_{i=1}^{N_{c,Eg5}} -f_i^{Eg5} \frac{O_{i,j}\phi_{i,j}}{\pi \ell_i} \exp\left(-\frac{L_i}{K d_{cent}}\right) \vec{m}_i, \tag{6}$$

$$\vec{F}_c^{HSET} = \sum_{i=1}^{N_{c,HSET}} -f_i^{HSET} \frac{O_{i,j}\phi_{i,j}}{\pi \ell_i} \exp\left(-\frac{L_i}{K d_{cent}}\right) \vec{m}_i, \tag{7}$$

respectively, where $\phi_{i,j}$ is the angle of intersection between MT i on centrosome c and MT j on centrosome k, L_i is the distance between the centrosome c to the point of force application on the i^{th} MT, d_{cent} is the distance between centrosomes c and k, and $O_{i,j}$ is the overlap distance of interpolar MTs i and j (Figure A2 B).

We calculate the angular velocities, η_i, η_j, and update the angle of interpolar MTs i and j by:

$$\vec{v_c} + \eta_i L_i \vec{n_i} + v_i \vec{m_i} = \vec{v_k} + \eta_j L_j \vec{n_j} + v_j \vec{m_j}, \tag{8}$$

where $\vec{n_i}, \vec{n_j}$ are the unit normal vectors to MTs i and j, respectively, $\vec{v}_c, \vec{v}_k$ are the velocities of centrosomes c and k, respectively, and v_i, v_j are the relative velocities between the protein (either Eg5 or HSET) and the i^{th} and j^{th} MT, respectively [64].

A.4 Spindle-Pole Dynein

In addition to its localization at the cell cortex, dynein is highly localized to spindle poles during mitosis, where it is necessary for the maintenance of MT minus-end focusing and spindle integrity [38, 39, 41]. We allow MTs nucleated from opposing centrosomes to have a probability $P_{d_{sp}} = 0.5$ of binding to this population of dynein if they get within a distance, $\mathcal{D}_{d_{sp}}$ from the center of the centrosome. This motor-MT interaction follows exactly equation (2). The force on centrosome c by dynein localized at spindle poles is calculated by:

$$F_c^{d_{sp}} = \sum_{i=1}^{N_{c,d_{sp}}} -f_i^{d_{sp}} \exp\left(-\frac{\ell_i}{K d_{cent}}\right) \vec{m}_i. \tag{9}$$

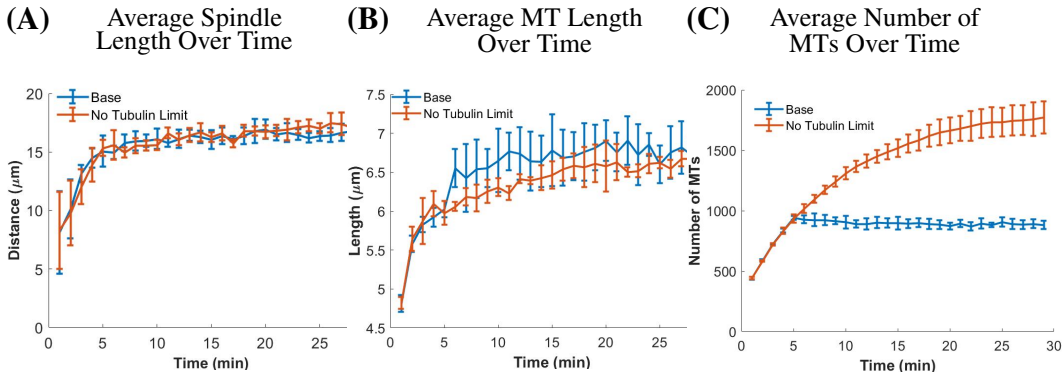

Figure A1: **Limiting tubulin impacts MT number but not spindle length or MT length.** Traces over time for the base case and case without limiting tubulin for spindle length (A), MT length (B), and MT number (C). Averages calculated for 10 simulations. Error bars are standard deviation.

B Cortical pushing, but not pulling, is required for centrosome centering during interphase

It has been well documented that cortical pushing and pulling forces position the centrosome in the center of the cell during interphase; the time between successive mitotic divisions when only one centrosome is present. The dynamics

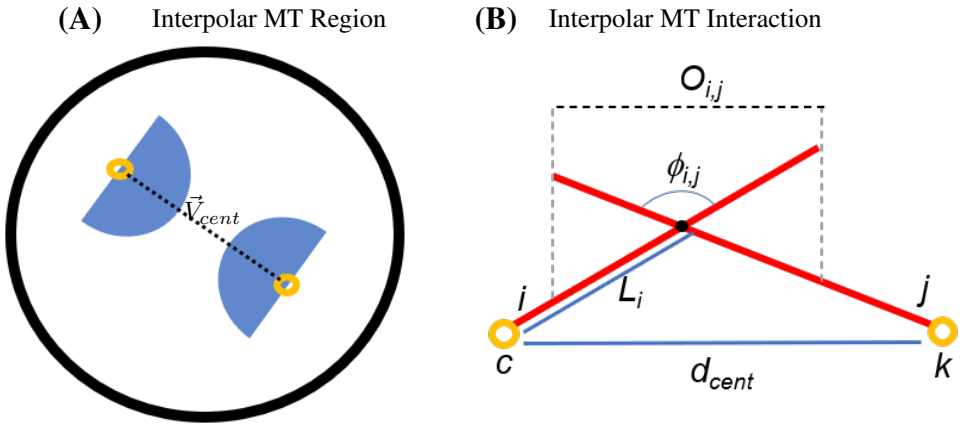

Figure A2: **Interpolar MTs.** (A) Schematic of interpolar MT region. Black dashed line indicates the vector between the centrosomes ($\vec{V}_{cent}$). Interpolar MTs are those that lie within the blue shaded regions. (B) Schematic of interpolar MT interaction. MTs i, j are nucleated from centrosomes c, k, respectively.

of centrosome centering has been shown in both cells [50] and microfabricated chambers [33, 34]. To confirm that our model captures appropriate centrosome dynamics, we observed centrosome movement over time with varying concentrations of cortical dynein, as has been experimentally tested *in vitro* [33]. All parameters are the same as those used in the base case and are listed in Table 2.

We show that a centrosome efficiently centers with our "intermediate" dynein concentration ($P_d = 0.5$); centering 82% of the time (Figure A3 B). Centering is defined by the centrosome achieving a distance of at least 4 μm from the center of the cell.

We show further that altering cortical dynein concentrations impacts centering efficiency. Increasing dynein concentrations ($P_d = 0.75$) prevents centrosome centering, as we have increased pulling towards the boundary of the cell (Figure A3 C). Additionally, high dynein concentrations increase average centrosome velocity (Figure A3 D).

Alternatively, preventing MT binding to cortical dynein ($P_d = 0$) improved centering efficiency, with centrosomes centering 100% of the time (Figure A3 A). Additionally, both the maximum centrosome velocity and the average centrosome velocity is increased compared to the intermediate dynein case (Figure A3 D). These results are consistent with [33], who show that, with moderate MT lengths, MT centering is most efficient with no dynein and least efficient with high dynein. Together these results indicate that our model is capturing appropriate centrosome movement driven by MT-cortex derived forces.

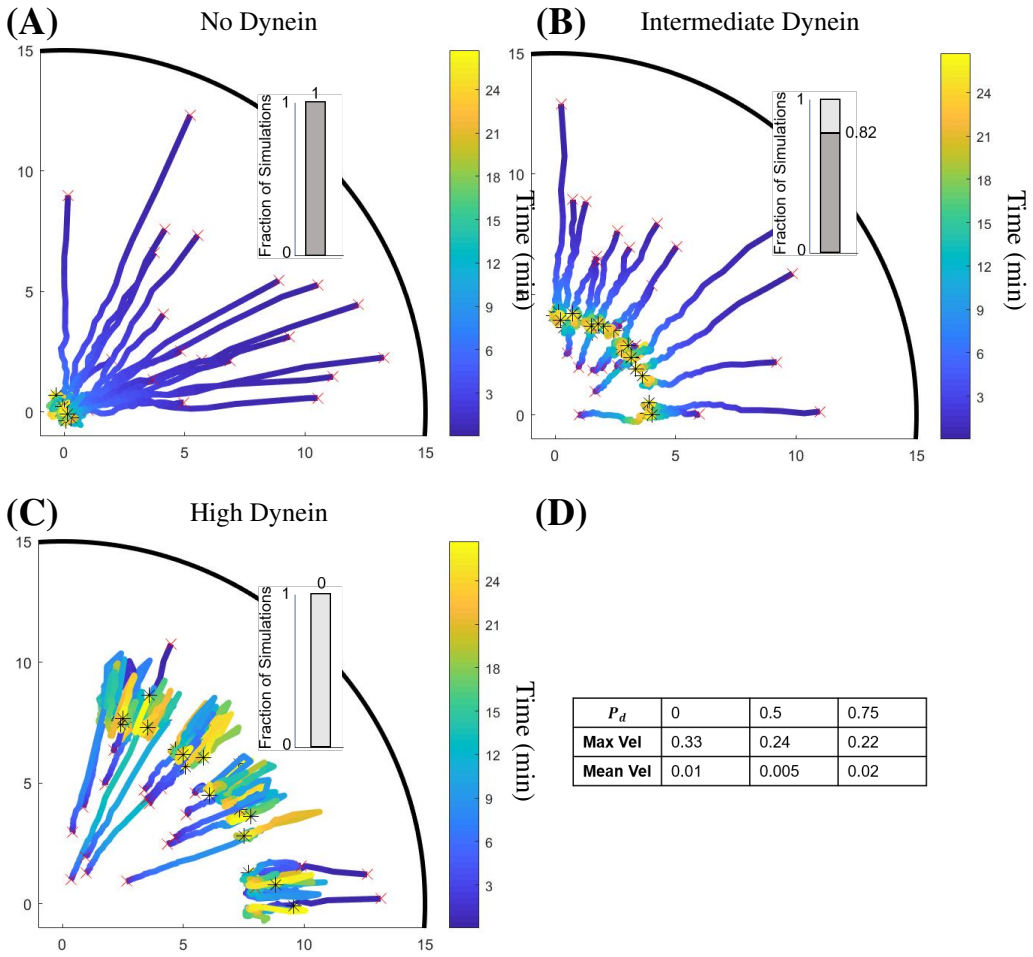

P_d	0	0.5	0.75
Max Vel	0.33	0.24	0.22
Mean Vel	0.01	0.005	0.02

Figure A3: **MT interactions with the cell cortex regulate centrosome movement and positioning.** (A) Centrosome movement traces over time with no MT binding to cortical dynein; $P_d = 0$ (B) Centrosome movement traces over time with MTs both binding to cortical dynein and pushing against the cell cortex; $P_d = 0.5$. (C) Centrosome movement traces over time with MTs binding to both cortical dynein and pushing against the cell cortex; $P_d = 0.75$. Bar plots represents the fraction of simulatons with the centrosome centered at the final time point. Dark gray bar represents centered centrosomes, light gray bar represented un-centered centrosomes. Red 'x' is initial centrosome position, black asterisk is final centrosome position. (D) Table showing the average maximum and mean centrosome velocities in the different conditions. All averages calculated from 50 simulations.

Table 2: Parameter Values

Parameter	Value	Description	Reference
Microtubules			
v_g	0.183 μms^{-1}	MT growth velocity (+ ends)	[56], [45]
v_s	0.3 μms^{-1}	MT shrinking velocity (− ends)	[45]
v_b	0.057 μms^{-1}	MT shrinking velocity (+ ends) bound to cortical dynein	[33]
v_f	0.0083 μms^{-1}	Poleward flux	[57]
k_1	0.167 s^{-1}	Rescue frequency	[45], [58]
κ	3.3 pNμm^2	Bending rigidity	[33]
f_{stall}	5 pN	Stall force of MTs	[59]
MT_{nuc}	2 s^{-1}	MT nucleation rate per centrosome	[60]
θ	$10\pi/180$	Slipping MT angle change	
M	6000 μm	Maximum sum of MT lengths	
Motor Proteins			
Dynein			
$f_{0,d}$	3.6 pN	Stall force of dynein	[61]
$v_{0,d}$	0.86 μms^{-1}	Walking velocity of dynein	[62], [61]
P_d	0.5	Probability of binding to cortical dynein	
$P_{d_{sp}}$	0.5	Probability of binding to spindle pole dynein	
$\mathcal{D}_d$	$4v_g(dt)$ μm	Distance required for binding to dynein	
$\mathcal{D}_{d_{sp}}$	1 μm	Distance required for binding to dynein at spindle poles	
Kinesin-5 (Eg5)			
$f_{0,Eg5}$	1.5 pN	Stall force of Eg5	[63]
$v_{0,Eg5}$	0.2 μms^{-1}	Walking velocity of Eg5	[64]
P_E	0.5	Probability of binding to Eg5	
Kinesin-14 (HSET)			
$f_{0,HSET}$	1.1 pN	Stall force of HSET	[65]
$v_{0,HSET}$	0.2 μms^{-1}	Walking velocity of HSET	[64]
P_H	0.5	Probability of binding to HSET	
$\mathcal{D}_{Eg5,HSET}$	$v_g dt$ μm	Distance required for binding to Eg5 or HSET	
Other			
c_r	0.3 μm	Radius of a centrosome	
$\mathcal{D}_r$	$2c_r$ μm	Distance for repulsive forces	
K	0.25	Scaling factor	
C	2 μm	Scaling for repulsive forces	
s	0.15 μm^{-1}	Scaling for catastrophe frequency	
μ	0.7 pNsμm^{-2}	Viscosity of the cytoplasm	[51]
γ	0.0012 μm^{-1}	Permeability of the cytoplasm	
ξ	20.6 pNs	Drag coefficient	